A novel tubulin inhibitor, 6h, suppresses tumor-associated angiogenesis and shows potent antitumor activity against non–small cell lung cancers

Received for publication, March 22, 2022, and in revised form, May 18, 2022 Published, Papers in Press, May 23, 2022,
https://doi.org/10.1016/j.jbc.2022.102063

Zi Liu[1,‡], Liancheng Huang[2,‡], Tianhao Zhou[1], Xing Chang[1], Yuying Yang[1], Yani Shi[1], Mingjing Hao[1], Zengqiang Li[1], Yingliang Wu[1], Qi Guan[2,*], Weige Zhang[2,*], and Daiying Zuo[1,*]

From the [1]Department of Pharmacology, and [2]Key Laboratory of Structure-Based Drug Design and Discovery, Ministry of Education, Shenyang Pharmaceutical University, Shenyang, China

Edited by Enrique De La Cruz

Tumor angiogenesis is closely associated with the metastasis and progression of non–small cell lung cancer (NSCLC), a highly vascularized solid tumor. However, novel therapeutics are lacking for the treatment of this cancer. Here, we developed a series of 2-aryl-4-(3,4,5-trimethoxy-benzoyl)-5-substituted-1,2,3-triazol analogs (6a–6x) as tubulin colchicine-binding site inhibitors, aiming to find a novel promising drug candidate for NSCLC treatment. We first identified 2-(2-fluorophenyl)-3-(3,4,5-trimethoxybenzoyl)-5-(3-hydroxyazetidin-1-yl)-2*H*-1,2,3-triazole (6h) as a hit compound, which inhibited angiogenesis induced by NSCLC cells both *in vivo* and *in vitro*. In addition, our data showed that 6h could tightly bind to the colchicine-binding site of tubulin and inhibit tubulin polymerization. We also found that 6h could effectively induce G2/M cell cycle arrest of A549 and H460 cells, inhibit cell proliferation, and induce apoptosis. Furthermore, we showed 6h had the potential to inhibit the migration and invasion of NSCLC cells, two basic characteristics of tumor metastasis. Finally, we found 6h could effectively inhibit tumor progression in A549 xenograft mouse models with minimal toxicity. Taken together, these findings provide strong evidence for the development of 6h as a promising microtubule colchicine-binding site inhibitor for NSCLC treatment.

Non–small cell lung cancer (NSCLC), a leading cause of cancer-related death worldwide, accounts for approximately 85% of all lung cancer cases (1–3). Despite the use of treatment options, such as chemotherapy, targeted therapy, or immunotherapy in the last decade, has resulted in steady improvement in survival for patients with NSCLC, anticancer drug resistance and metastasis are still the main reasons for the failure of treatment (4–6).

NSCLC is a solid tumor that is highly vascularized. Studies have shown that the growth and metastasis of solid tumors are supported by angiogenesis (7, 8). It is known that tubulin inhibitors are the main drugs for the treatment of NSCLC, with the effect of altering microtubule dynamics and inhibiting angiogenesis (9). Notably, colchicines and colchicine-binding site agents could inhibit solid tumor growth with the induction of apoptosis by disrupting the tumor neovasculature (10). Colchicine can bind to soluble β-tubulin at the α/β-tubulin interface and blunt the addition of GTP-bound α/β-tubulin dimers to the plus-end of polymerized microtubules. After colchicine binding to tubulin, the straight conformation of the α/β-tubulin heterodimeric subunit becomes curved, and this steric clash inhibits microtubule assembly (11). Because of the severe side effects (*e.g.*, colchicine), poor drug solubility (*e.g.*, combretastatin A4), and insufficient potency (*e.g.*, verubulin), colchicine-binding site agents have not been approved for cancer therapy so far (12). Thus, developing novel, safe, and highly efficacious colchicine-binding site agents to treat NSCLC is of paramount urgency.

Miller's laboratory first identified a novel colchicine-binding site agent, 4-substituted methoxybenzoyl-aryl-thiazole (SMART), whose molecular structure consists of a trimethoxybenzene ring, a five-membered heterocycle, a benzene ring substituted by different substituents, and a linker part (Fig. 1*A*) (13). Although SMART has shown promising anticancer activity by inhibiting microtubule polymerization, poor aqueous solubility and bioavailability have prevented its use for further development (14). In the previous research work, our group obtained a series of SMART analogs with 1,2,3-triazole as the B-ring, which are expected to retain potent tumor proliferation inhibitory activity and obtain metabolic stability *in vivo*. However, in the subsequent experiments, we found that these compounds were meaningless for the further investigation because of the poor solubility in addition to 2-aryl-4-(4-methylbenzoyl)-2*H*-1,2,3-triazoles (**Z**), which could overlap well with *N*-deacetyl-*N*-(2-mercaptoacetyl)–colchicine in the binding pocket (Fig. 1*A*). In addition, there was a tolerant region located near the C5 position of B-ring in compound **Z**, which was mainly composed of amino acid residues, such as AlA-100, ASN-101, ASN-249, and LYS-254 (Fig. 1*B*). We envisaged to retain a basic skeleton and

‡ These are co-first authors and contributed equally to this work.
* For correspondence: Daiying Zuo, zuodaiying@163.com; Weige Zhang, zhangweige2000@sina.com; Qi Guan, guanqi@syphu.edu.cn.

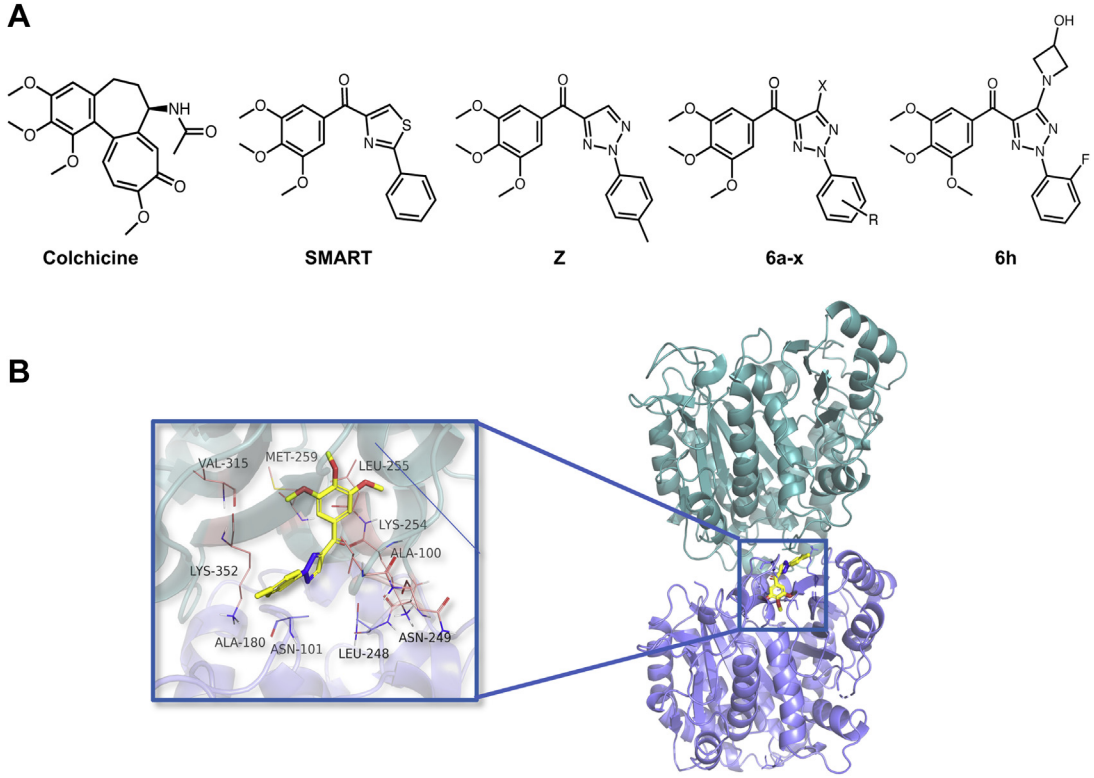

Figure 1. The structures of CBSIs that we studied and molecular docking model of compound Z and tubulin. *A*, structures of reported CBSIs (colchicine, SMART) and designed new CBSIs (**Z**, **6a–6x**). *B*, the binding mode of compound **Z** with tubulin. *Yellow sticks* show the structure of **Z**. The α-tubulin chains are shown in *pale purple*, whereas β-tubulins are colored in *pale cyan*. CBSI, colchicine-binding site inhibitor.

introduced polar structural fragments at the C5 position of the B-ring of compound **Z**, which could bind to the tolerant region with the aim of further enhancing the aqueous solubility of the whole molecule and maintaining good tumor proliferation inhibitory activity.

Here, a series of 2-aryl-4-(3,4,5-trimethoxy-benzoyl)-5-substituted-1,2,3-triazol analogs (**6a–6x**) were initially reported as novel colchicine-binding site agents. A structure–activity relationship study was utilized to screen the hit compound 2-(2-fluorophenyl)-3-(3,4,5-trimethoxybenzoyl)-5-(3-hydroxy azetidin-1-yl)-2*H*-1,2,3-triazole (**6h**). We found that **6h** exhibited potent antitumor, antimetastatic, and anti-angiogenic effects, suggesting its potential use as a therapeutic agent with multiple inhibitory effects on NSCLC angiogenesis and growth.

Results

Synthesis and verification of target compounds

The general method for the synthesis of 2-aryl-4-(3,4,5-trimethoxy-benzoyl)-5-substituted-1,2,3-triazol analogs (**6a–6x**) was illustrated in Figure 2. Briefly, methyl 3,4,5-trimethoxybenzoate (**1**) and acetonitrile were used as starting materials in the presence of sodium hydride to afford 3-oxo-3-(3,4,5-trimethoxyphenyl) propanenitrile (**2**). To obtain substituted diazonium salts (**4**), corresponding phenylamine (**3**) was used (15). Next, the diazonium salt of different aromatic amines and **2** were used by a coupling reaction to obtain a diverse range of hydrazone derivatives (**5**). Finally, a tandem nucleophilic addition of alkylamines to hydrazonoyl cyanides and *in situ* oxidative cyclization in the presence of copper (II) and air generated the desired compounds **6a–6x** (Fig. 2).

The compounds were characterized using ^{1}H NMR, ^{13}C NMR, and mass spectrometry (relative strength index), and their purity was determined by reverse-phase HPLC. The data of generated spectrum were loaded into the supporting information.

Antiproliferative activity studies in vitro *and physicochemical properties of compounds*

The antiproliferative activities of target compounds **6a–6x** were evaluated in A549, SGC-7901, and MCF-7 cells by the 3-(4,5-dimethylthiazol-2-yl)-2,5-diphenyl-2H-tetrazolium bromide (MTT) assay: colchicine and SMART were used as positive controls. The IC_{50} values of the compounds are shown in Table 1. Our previous findings suggested that the introduction of a substituent at the C5 position of the B-ring (1,2,3-triazole) may improve the *in vitro* antiproliferative activity and aqueous solubility of compounds. Therefore, in this study, we focused on introducing different groups at the C5 position of the B-ring to improve the aqueous solubility and screen out compounds with stronger antitumor activity. As depicted in

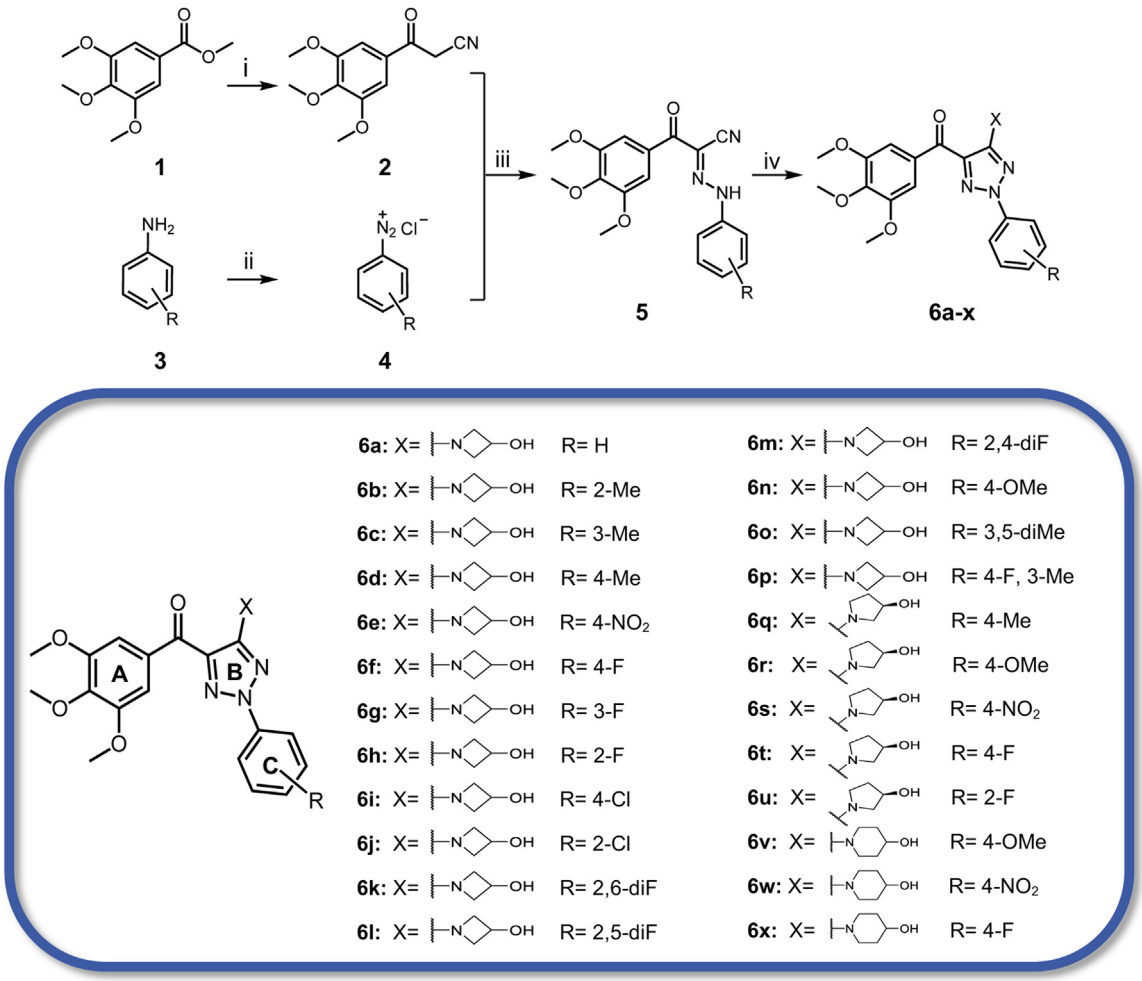

Figure 2. Synthetic routes of 6a–6x. Reagents and conditions: (i) CH_3CN, NaH (60%), reflux, 3 h; (ii) aqueous HCl (6 M), $NaNO_2$, H_2O, 0 °C, 30 min; (iii) NaOAc, EtOH/H_2O, 0 °C at room temperature, 1 h; and (iv) amines, $Cu(AcO)_2$, CH_3CN, reflux, 5 to 8 h.

Table 1, most compounds showed potent antiproliferative activity at submicromolar or nanomolar concentrations against the three different human tumor cells.

The structure–activity relationship of **6a–6x** has been further discussed according to the preliminary screening results of MTT. First, we introduced a six-membered ring (4-hydroxypiperidin-1-yl) at C5 position of the B-ring, and when the substituent on the C-ring was an electron-donating group or an electron-withdrawing group like methoxyl (**6v**), nitro (**6w**), fluoro (**6x**), no significant difference in the antiproliferative activity of the compounds was observed. Similarly, when we introduced a five-membered ring (3-hydroxypyrrolidin-1-yl) at C5 position of B-ring, the compounds (**6q–6u**) still did not show potent antiproliferative activity. In addition, replacement of the electron-donating groups (methyl [**6q**] or methoxyl [**6r**]) at C-ring by electron-withdrawing groups (nitro [**6s**] or fluoro [**6t**, **6u**]) tended to reduce the activity. When the four-membered ring (3-hydroxyazetidin-1-yl) was used as the C5 substituent of B-ring, the activity was greatly improved (**6u** and **6h**). Meanwhile, the introduction of fluoro group (**6h** and **6m–6k**) at C2 position of C-ring could strengthen the inhibitory activities toward three cancer cell lines. In summary, the antiproliferative activity of derivatives with 3-hydroxyazetidin-1-yl group at C5 position of B-ring was better than that with 3-hydroxypyrrolidin-1-yl group and 4-hydroxypiperidin-1-yl group, and the introduction of fluoro group onto C2 position of C-ring further enhanced the anticancer activity. Therefore, **6h** was selected as the hit compound for further evaluation based on its promising *in vitro* activity.

To further validate the rationality of design strategy, cLogP, polar surface area, hydrogen-bond acceptor atoms, and hydrogen-bond donor atoms of **6a–6x**, **Z**, and SMART were calculated using Discovery Studio 3.0 software (BIOVIA) and Molinspiration online software (https://www.molinspiration.com/), respectively. The results showed that the introduction of hydrophilic group at the C5 position of B-ring could increase the water solubility of **6h** (Table 2).

6h suppresses angiogenesis of NSCLC in vitro *and* in vivo

According to previous studies, tumor-associated angiogenesis provides the necessary conditions for the growth and development of solid tumors (7, 8). To directly measure the effects of **6h** on angiogenesis of NSCLC, we first prepared

Table 1
In vitro antiproliferative activities of the target compounds 6a–6x

Compound	IC_{50} (μM)		
	A549	SGC-7901	MCF-7
6a	9.34	3.16	0.219
6b	0.292	0.285	1.06
6c	1.45	1.06	0.542
6d	0.850	>10	0.106
6e	1.04	0.272	0.244
6f	17.7	>30	0.219
6g	0.985	0.126	0.257
6h	0.063	0.120	0.094
6i	0.211	0.117	0.130
6j	2.42	0.535	1.74
6k	4.26	1.68	1.99
6l	0.755	0.098	0.497
6m	0.150	0.120	0.116
6n	2.05	2.48	1.41
6o	1.43	2.78	0.999
6p	5.99	7.69	4.90
6q	0.848	0.570	0.324
6r	1.15	1.08	0.194
6s	>30	0.595	4.21
6t	0.825	1.07	0.203
6u	>30	2.93	3.10
6v	0.496	3.25	4.94
6w	0.932	0.964	2.01
6x	5.06	0.394	4.68
Colchicine[a]	0.107	0.043	0.059
SMART[a]	0.089	0.019	0.048

[a] Used as positive controls.

NSCLC cells (A549 and H460) conditioned medium (CM) to simulate the tumor microenvironment (Fig. 3*A*). HMEC-1 (human microvascular endothelial cell line) cells were pretreated with the prepared A549 or H460 CM for tube formation assay, a rapid quantitative *in vitro* angiogenesis assay that is commonly used to assess the antiangiogenic effect of compounds (16). Tube formation refers to the connection of existing vasculature to new blood vessels through the extracellular matrix. To simulate this process *in vitro*, endothelial cells are grown in culture medium and then placed on Matrigel to examine their angiogenesis properties. Drugs inhibit angiogenesis by inhibiting tube formation or disrupting the formed tubules. The effect of the drug on tube formation is usually quantified by counting the number of connections between tubules and the length of tubules (17). Our data showed that elongated and robust capillary-like structure formation was observed in both A549 or H460 CM-stimulated groups and control groups, with significantly longer tube lengths in A549 or H460 CM-stimulated groups (Fig. 3*B*). However, **6h** could effectively interfere with the formation of capillary-like structures, resulting in imperfect tubes (Fig. 3*B*).

Endothelial cell proliferation, migration, and tubular formation are several key stages of angiogenesis, which can be simulated by the rat aortic ring experiment (18). In this experiment, aortic rings embedded in Matrigel and cultured under chemically defined conditions produce dendritic vascular growths, which can be stimulated or inhibited by angiogenesis modulators (19). The effect of **6h** on microvessel sprouting was examined in a rat aortic ring angiogenesis model. As shown in Figure 3*C*, the formation of microvascular networks surrounding the aortic ring was markedly triggered by A549 or H460 CM compared with the control group. Consequently, the new vessel emerging from the aortic ring induced by A549 or H460 CM was significantly suppressed by increasing concentrations of **6h**.

It has been shown that chicken chorioallantoic membrane (CAM) develops from a small avascular membrane to a structure covering the entire inner surface of the shell in a very short period, displaying a densely organized vascular network (20). Because of its rapid vascular growth, the CAM has been proved to be a unique model for studying the process of neovascularization and the effects of antiangiogenic agents *in vivo* (21). The efficacy of antiangiogenic agents is assessed based on the quantification of vessel density, vessel branching points, and vessel length (22). Therefore, the CAM assay was also performed to verify the effect of **6h** on neovascularization. We found that more new blood vessels formed in A549 or H460 CM-stimulated groups compared with the control groups (Fig. 3*D*). As the dose of **6h** increased, microvascular entanglement was observed and newly formed blood vessels were obviously blocked, suggesting that **6h** inhibited CAM angiogenesis (Fig. 3*D*).

Table 2
Prediction of physicochemical properties of compounds 6a–6x, Z, and SMART

Compound	cLogP	PSA	HBA	HBD
6a	1.90	98.86	8	1
6b	2.51	98.86	8	1
6c	2.51	98.86	8	1
6d	2.34	98.86	8	1
6e	1.85	144.78	10	1
6f	2.06	98.86	8	1
6g	2.25	98.86	8	1
6h	2.22	98.86	8	1
6i	2.57	98.86	8	1
6j	2.74	98.86	8	1
6k	2.55	98.86	8	1
6l	2.57	98.86	8	1
6m	2.36	98.86	8	1
6n	1.95	108.19	9	1
6o	3.14	98.86	8	1
6p	2.65	98.86	8	1
6q	2.62	98.86	8	1
6r	2.22	108.19	9	1
6s	2.12	144.78	10	1
6t	2.33	98.86	8	1
6u	2.49	98.86	8	1
6v	1.76	108.19	9	1
6w	1.66	144.78	10	1
6x	1.86	98.86	8	1
Z	2.90	75.49	6	0
SMART	4.11	57.66	5	0

cLogP, calculated logarithm of octanol–water partition coefficient; HBA, hydrogen-bond acceptor atoms; HBD, hydrogen-bond donor atoms; PSA, polar surface area.

6h inhibits the proliferation of cancer cells in vitro *and displays potential in the treatment of NSCLC*

We evaluated the effect of **6h** on proliferation of a variety of cancer cell lines by the MTT assay, and colchicine was served as positive control. As shown in Table 3, **6h** showed better antiproliferative activity than colchicines, especially in cancer cell lines like BEL-7402, MCF-7/ADM, A549, A549/Taxol, and H460. Among which, **6h** exhibited the highest cytotoxicity against human NSCLC cell lines. IC_{50} values of **6h** to A549 and H460 cells were 62.59 ± 7.08 and 88.70 ± 10.54 nM,

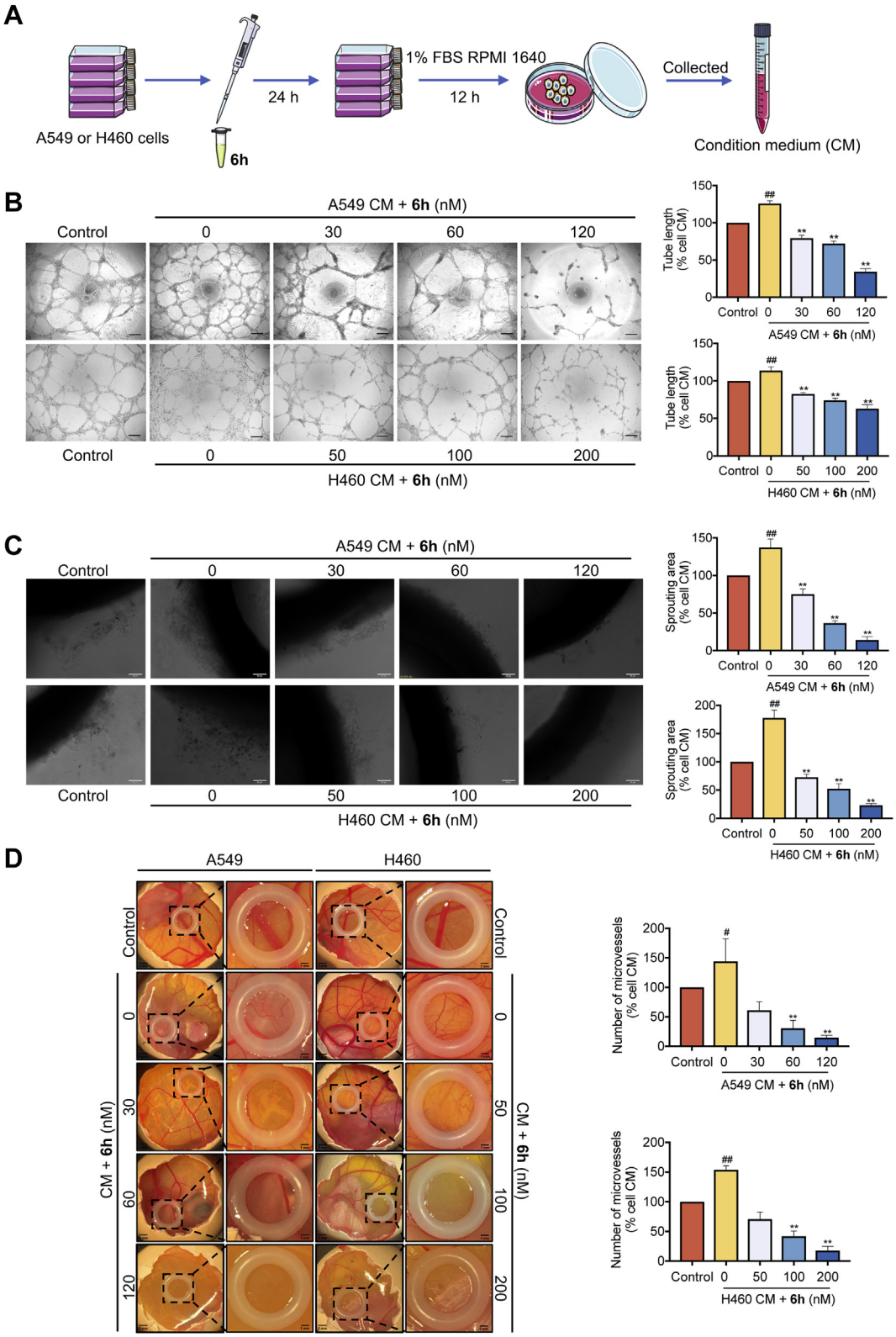

Figure 3. Effects of 6h on NSCLC cell–induced angiogenesis *in vitro* and *in vivo*. *A*, preparation of conditioned medium (CM). *B*, the tube formation ability of HMEC-1 cells cultured by CM, which was collected from A549 cells pretreated with **6h** (0, 30, 60, or 120 nM) or H460 cells pretreated with **6h** (0, 50, 100, or 200 nM) was tested by the endothelial cell tube formation assay. The scale bar represents 200 μm. *C*, the rat aortic ring microvessel sprouting induced by CM, which was collected from A549 cells pretreated with **6h** (0, 30, 60, or 120 nM) or H460 cells pretreated with **6h** (0, 50, 100, or 200 nM) was tested by rat aortic ring assay. The scale bar represents 50 μm. *D*, effect of **6h** on the angiogenesis was tested by chicken chorioallantoic membrane (CAM) assay. Data are presented as mean ± SD. $^{\#}p < 0.05$ and $^{\#\#}p < 0.01$ *versus* control group, $^{**}p < 0.01$ *versus* A549 or H460 CM group. HMEC, human microvascular endothelial cell line; NSCLC, non–small cell lung cancer.

Table 3
IC_{50} of 6h against various human cancer cell lines (mean ± SD, n = 3)

Tumor type	Cell line	IC_{50} (nM)	
		6h	Colchicine
Stomach	SGC-7901	120.41 ± 13.01	42.56 ± 5.41
Liver	BEL-7402	116.71 ± 21.37	137.69 ± 19.98
	HepG2	65.36 ± 8.93	40.06 ± 4.43
Breast	MCF-7	94.18 ± 12.82	58.87 ± 5.69
	MCF-7/ADM	8380.37 ± 202.75	54,480.10 ± 531.10
	MDA-MB-231	760.95 ± 38.56	237.83 ± 22.51
Lung	A549	62.59 ± 7.08	107.37 ± 14.11
	A549/Taxol	462.17 ± 39.02	6729.50 ± 498.10
	H460	88.70 ± 10.54	150.21 ± 16.03
Colon	HT-29	296.44 ± 43.18	92.63 ± 11.72

respectively. Therefore, A549 and H460 cells were selected for the following research.

Next, Figure 4, *A* and *B* showed that **6h** effectively inhibited the proliferation of both NSCLC cell lines in time- and concentration-dependent manners. Meanwhile, the results of colony formation assay confirmed that **6h** had a robust growth inhibitory effect on A549 and H460 cells compared with control group (Fig. 4*C*). Together, these data demonstrated that **6h** suppressed the proliferation of A549 and H460 cells.

6h disrupts microtubule polymerization

To investigate whether the anticancer effect of **6h** is related to microtubules, molecular docking studies were used to predict the direct interaction between **6h** and *N*-deacetyl-*N*-(2-mercaptoacetyl)–colchicine (Protein Data Bank [PDB] ID: 1SA0). As shown in Figure 5*A*, the positions of colchicine, **Z**, and **6h** in the colchicine-binding pocket were similar, and the molecular skeletons of these three molecules could be superimposed well. In addition, the binding sites of **6h** with the pocket consist of LEU-255, LEU-248, MET-259, LYS-352, ALA-180, and other amino acid residues, which were consistent with colchicine and **Z**. The benzene ring of **6h** could form σ–π conjugated interactions with LEU-255 and LEU-248, which contribute greatly to the stability of small molecules in protein active pockets. Notably, the active groups at both ends of **6h** could form hydrogen bonds with amino acids. The hydrogen bond distance was short, with an average length of

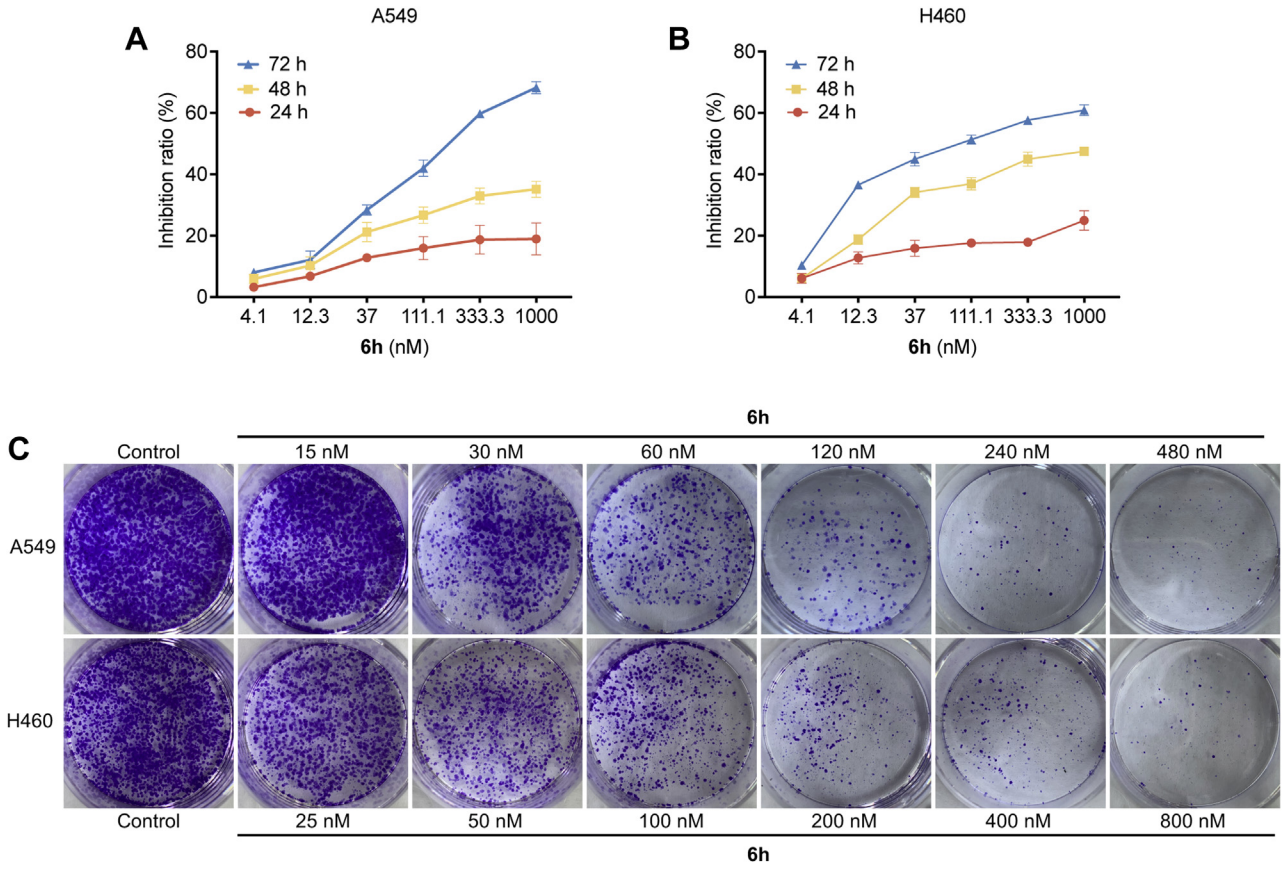

Figure 4. Antiproliferative activity screening of 6h *in vitro*. Cell inhibition ratio was determined by the MTT assay in A549 cells (*A*) and H460 cells (*B*) treated with **6h** (0–1000 nM) for 24, 48, or 72 h. *C*, the antiproliferative effects of **6h** at 0.25 IC_{50}, 0.5 IC_{50}, IC_{50}, 2 IC_{50}, 4 IC_{50}, and 8 IC_{50} on A549 and H460 cells were measured by colony formation assay. MTT, 3-(4,5-dimethylthiazol-2-yl)-2,5-diphenyl-2H-tetrazolium bromide.

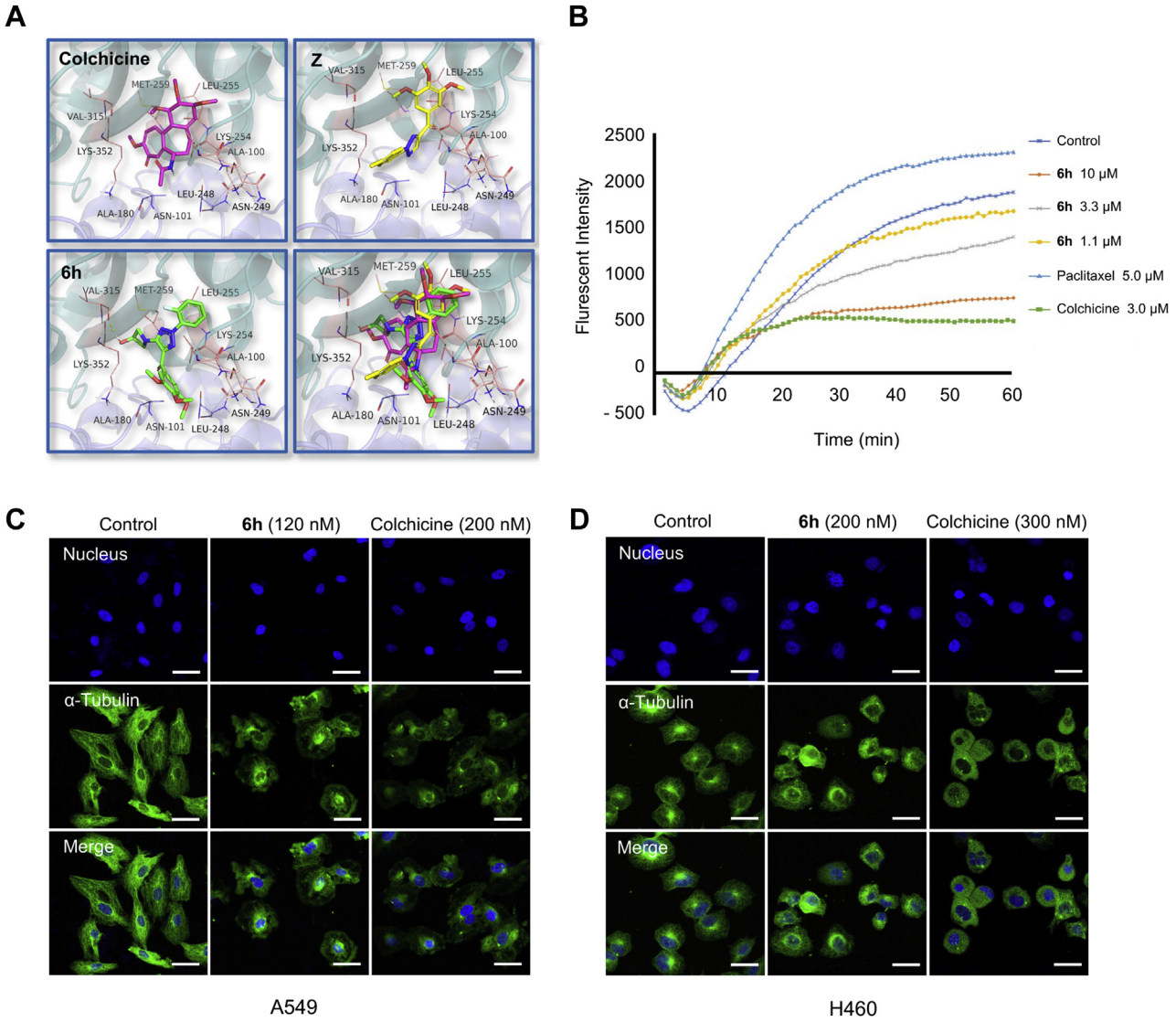

Figure 5. 6h inhibits microtubule polymerization *via* binding to colchicine-binding site of tubulin. *A*, proposed binding modes for **6h** in comparison with colchicine and **Z** at the colchicine site. Carbon atoms are shown in *salmon* for colchicine, *yellow* for **Z**, and *green* for **6h**. The residues from the α-tubulin chain are shown in *pale purple*, whereas residues from β-tubulin are colored in *pale cyan*. *B*, the effect of **6h** on tubulin polymerization was measured by Tubulin Polymerization Assay Kit. Tubulin was preincubated for 1 min with **6h** at 1.1, 3.3, and 10 μM, colchicine at 3.0 μM, paclitaxel at 5.0 μM, or vehicle DMSO. *C*, A549 cells were treated with **6h** (120 nM) or colchicine (200 nM) for 24 h. *D*, H460 cells were treated with **6h** (200 nM) or colchicine (300 nM) for 24 h, respectively. After incubation, microtubules were labeled with anti–α-tubulin antibody and FITC-conjugated secondary antibody (*green*), the nuclei were stained with DAPI (*blue*), and the microtubules were observed by confocal microscopy. The scale bar represents 10 μm. DAPI, 4′,6-diamidino-2-phenylindole; DMSO, dimethyl sulfoxide; MTT, 3-(4,5-dimethylthiazol-2-yl)-2,5-diphenyl-2H-tetrazolium bromide.

2.8 Å, which was much smaller than the 3.5 Å of traditional hydrogen bond. These strong interactions could effectively improve the stability of **6h** in the colchicine activity pocket of tubulin. In summary, **6h** may exhibit its biological activity by binding to tubulin at the colchicine-binding site.

Subsequently, we conducted the *in vitro* microtubule polymerization assay to evaluate the effect of **6h** on assembly properties of tubulin at the molecular level. Purified and unpolymerized tubulin was assembled in the presence of GTP and magnesium ions, and the fluorescence intensity was detected to become stronger with time, indicating the occurrence of tubulin polymerization. In our study, colchicine promoted microtubule depolymerization and paclitaxel enhanced microtubule polymerization compared with the control group, respectively. Our data showed that **6h** could promote the depolymerization of purified microtubulin in a concentration-dependent manner, which further confirmed that **6h** was a novel tubulin-depolymerizing agent (Fig. 5*B*).

Since microtubule protein polymerization and microtubule assembly play critical roles in maintaining cell morphology and essential cellular functions (23), immunofluorescence analysis was performed to reveal whether **6h** disrupts microtubule dynamics in NSCLC cells. Figure 5, *C* and *D* showed that the microtubule network of A549 or H460 cells in the control group was seen clearly with filamentous microtubules neatly arranged around the nucleus. In contrast, the organized cytoskeleton was destroyed in **6h**-treated cells, resulting in rounding cells, which were similar to colchicine. Collectively,

our data suggested that **6h** significantly interferes with mitosis and inhibits microtubule protein polymerization in NSCLC cells, which may ultimately lead to tumor cell death.

6h evokes G2/M cell cycle arrest in A549 and H460 cells

There is evidence that drugs targeting microtubules usually induce cell cycle arrest (24, 25). Since we have demonstrated that microtubule protein polymerization was disrupted by **6h**, further experiments were necessary to investigate the effect of **6h** on the cell cycle of NSCLC cells. Figure 6*A* showed that the proportion of G2/M phase A549 cells was increased in a time-dependent manner (0–12 h) after **6h** (120 nM) treatment, indicating that **6h** could induce G2/M phase cell cycle arrest. Similarly, **6h** (200 nM) evoked G2/M cell cycle arrest of H460 cells in a time-dependent manner (0–24 h) (Fig. 6*B*). Especially, the decrease in the percentage of cells at G2/M phase was accompanied by a significant increase at the subG1 phase, indicating the initiation of apoptosis.

6h induces apoptosis in NSCLC cells

Mitotic arrest of cancer cells induced by microtubule-targeting agents is usually accompanied by apoptosis (9). We next explored whether **6h** could induce apoptosis in NSCLC cells. Hoechst 33258 staining assay showed that the morphological shrinkage of chromatin with vivid blue fluorescence appeared in A549 and H460 cells following the treatment of **6h**, suggesting NSCLC cells undergo apoptosis (Fig. 7*A*). Moreover, the effect of **6h** on apoptosis was detected by annexin V–FITC/propidium iodide (PI) double staining. The results showed that **6h** treatment (120 nM or 200 nM) could increase the proportion of apoptosis in A549 and H460 cells time dependently (Fig. 7*B*).

Members of the family of cysteine-aspartic proteases (caspases) play a vital role in the initiation and execution of apoptosis (9). Among them, caspase 8 and caspase 9 are usually responsible for activating the caspase cascade reaction followed by caspase 3 as the main executor of apoptosis, which ultimately triggers nuclear fragmentation. The poly(ADP-ribose) polymerase (PARP) is the main cleavage target of caspase 3, and the cleavage of which is considered to be an indicator of caspase 3 activation (9). In order to understand the molecular mechanism of **6h**-induced apoptosis, the expression levels of related proteins were determined by Western blot analysis. As shown in Figure 7*C*, **6h** (120 nM) could significantly increase cleaved-PARP, p53, cleaved-caspase 8, FAS, and cleaved-caspase 3 protein expression in time-dependent manners but barely had effect on the expression of cleaved-caspase 9 and Bax in A549 cells. Similarly, **6h** (200 nM) time-dependently upregulated the expression of cleaved-

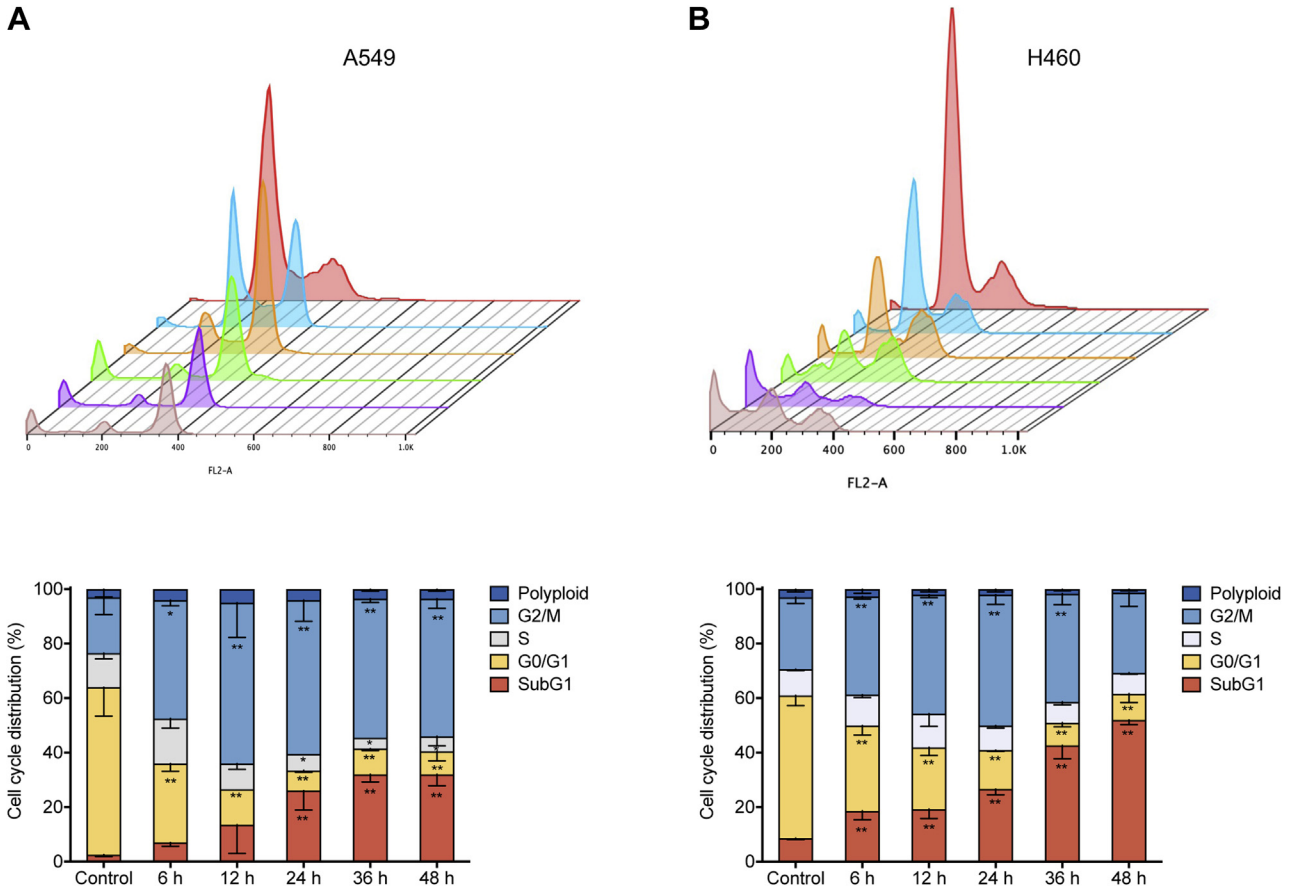

Figure 6. 6h treatment induces A549 and H460 cell cycle arrest at G2/M phase in time-dependent manners. A549 cells (*A*) or H460 cells (*B*) were treated with **6h** (2 IC_{50}) for indicated time (0, 6, 12, 24, 36, or 48 h), and the percentage of cells in specific cell cycle phase was quantified. *$p < 0.05$, **$p < 0.01$ *versus* control.

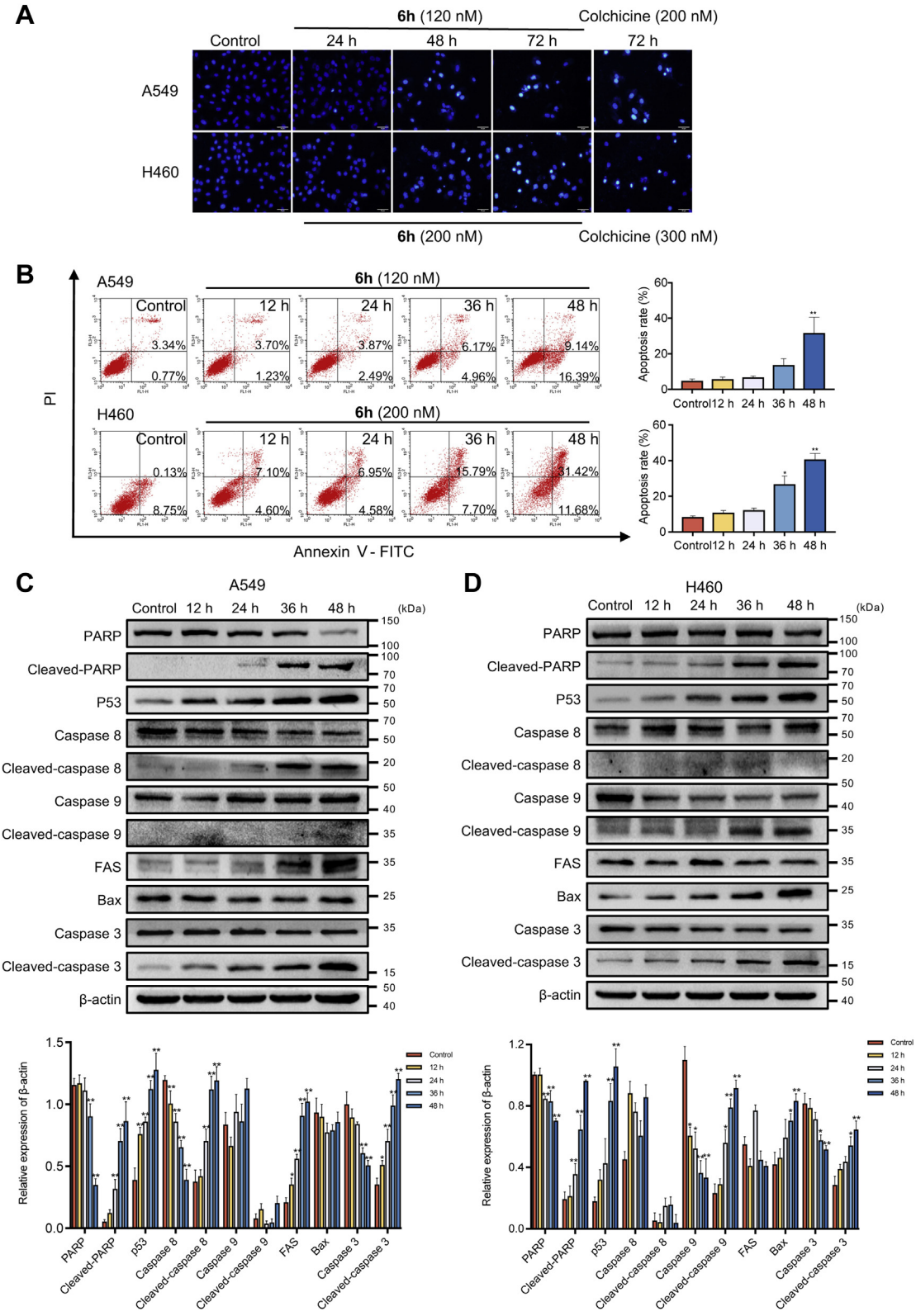

Figure 7. 6h induces apoptosis in A549 and H460 cells. *A*, A549 and H460 cells were treated with **6h** (2 IC_{50}) or colchicine (2 IC_{50}) for 24, 48, or 72 h, and then the nuclei were stained with Hoechst 33258, and photographed by Olympus inverted fluorescence microscope. The scale bar represents 50 μm. *B*, the apoptosis of A549 and H460 cells treated with **6h** (2 IC_{50}) for 12, 24, 36, or 48 h was measured by flow cytometry with annexin V–FITC staining. The percentage of apoptosis rate in A549 and H460 cells was quantified. Changes of the expression of cell apoptosis–related proteins in A549 cells (*C*) or H460 cells (*D*) treated with **6h** (2 IC_{50}) for indicated time (0, 12, 24, 36, or 48 h) were measured. The histogram in each panel indicated the relative band intensity generated form densitometric scans of three independent experiments on arbitrary densitometric units. $^{*}p < 0.05$, $^{**}p < 0.01$ *versus* control.

PARP, p53, cleaved-caspase 9, Bax, and cleaved-caspase 3 in H460 cells, whereas the expression of cleaved-caspase 8 and FAS had no change (Fig. 7*D*). These results proved that the apoptosis of NSCLC cells induced by **6h** was caspase dependent.

6h inhibits motility in NSCLC cells

Metastasis is a major cause of poor life quality and survival rate of patients with NSCLC (26). In this work, we explored whether **6h** could inhibit the migration and invasion of NSCLC cells by wound-healing and transwell assays, respectively. The results showed that **6h** apparently reduced the migration distance of A549 and H460 cells in concentration-dependent manners (Fig. 8*A*). As the concentration of **6h** increased, the number of cells crossing the transwell membrane was decreased significantly, indicating that **6h** could inhibit the migration and invasion ability of A549 and H460 cells (Fig. 8, *B* and *C*). Local tumor invasion is one of the earliest stages of tumor metastasis, in which the degradation of basement membrane is the key event (27). The extracellular matrix degradation ability of matrix metalloproteinase 2 (MMP-2) and MMP-9 is closely associated with tumor cell metastasis (27). Therefore, the effect of **6h** on the expression levels of MMP-2 and MMP-9 proteins was examined by Western blot assay. As expected, the results clearly demonstrated that MMP-2 and MMP-9 expression levels were decreased after **6h** treatment in A549 and H460 cells (Fig. 8, *D* and *E*). These data revealed that **6h** had the potential to inhibit the metastasis of NSCLC cells.

6h significantly suppresses the growth of xenograft NSCLC and angiogenesis

Based on the findings *in vitro*, the NSCLC xenograft nude mouse model was established to further explore the antitumor effect of **6h** *in vivo*. The vehicle, colchicine (0.5 mg/kg), or **6h** (3, 10, or 30 mg/kg) was injected (i.p.) every other day since the tumor volume grew to 200 mm^3. After 15 days of treatment, the mice were sacrificed and the tumors were removed (Fig. 9*A*). The treatment of **6h** or colchicine effectively inhibited tumor growth compared with the model group (Fig. 9, *B* and *C*). Figure 9*D* showed that there was no obvious change in body weight for 13 days between **6h**-treated groups and the model group, whereas decreased body weight was observed in colchicine-treated groups from ninth of treatment. H&E staining showed little detectable pathologic abnormalities in heart, liver, spleen, lung, or kidney between the **6h**-treated groups and the model group (Fig. 9*E*). However, colchicine was found to be more nephrotoxic than **6h**, suggesting that **6h** has advantage in drug safety compared with colchicine.

In addition, the immunohistochemical assay was used to detect the expression of Ki67 (marker of proliferation), TUNEL-positive cells, and the expression of angiogenic marker CD31 in order to further confirm the effect of **6h** on cell proliferation, apoptosis, and tumor vasculature. Figure 9*F* showed that the expression of Ki67 was significantly reduced by **6h** treatment compared with model group, indicating that **6h** had the ability to inhibit tumor proliferation in tumor-bearing nude mice. Simultaneously, the result of TUNEL staining also showed that the TUNEL-positive cells were significantly increased in **6h** or colchicine-treated tumor, suggesting that **6h** could promote apoptosis *in vivo*. Furthermore, immunohistochemical staining showed that the density of microvessels with CD31 staining was greatly decreased in response to the treatment with **6h** or colchicine (Fig. 9*F*). The aforementioned results were further verified by Western blot (Fig. 9*G*). In particular, we observed upregulation of cleaved-caspase 3, which is considered a key indicator of apoptosis. Overall, **6h** could exert antitumor effects by inhibiting tumor growth, inducing tumor tissue apoptosis, and targeting tumor vasculature without obvious toxicity.

Discussion

Antiangiogenesis therapy is a promising strategy for the treatment of NSCLC. However, the existing antiangiogenic drugs have limited clinical application because of their drug resistance and adverse reactions (6). Therefore, the development of high-efficiency and low-toxic chemotherapeutic drugs with simultaneous inhibition of tumor angiogenesis and direct cytotoxicity is promising. Here, we first reported a novel colchicine site microtubule depolymerization agent **6h**. Our *in vitro* and *in vivo* results proved that **6h** could play an anti-NSCLC effect by inducing cell apoptosis and targeted destruction of tumor vasculature (Fig. 10).

Recent years, researchers are committed to developing new colchicine-binding site inhibitors with different scaffolds. 1,2,3-Triazoles have been favored in drug design because of their broad range of pharmacotherapeutic effects (28). Such heterocycles have high dipole moments and are capable of forming hydrogen bonds, which may facilitate binding to biomolecules (28). In this study, we designed, synthesized, and evaluated 24 target compounds. The MTT assay and software calculations confirmed that most of the compounds had excellent ability to inhibit cell viability. Meanwhile, we found that the antiproliferative activity of the derivatives introducing 2-hydroxyazetidin-1-yl at the C5 position was better than that of the derivatives introducing 3-hydroxypyrrolidin-1-yl and 4-hydroxypiperidin-1-yl. Finally, we chose **6h**, the most active one, for more in-depth exploration.

Previous studies have confirmed that the anticancer activity of some microtubule inhibitors targeting the colchicine site *in vitro* and *in vivo* is mediated by antiangiogenesis (11). The anticancer activity of tanshinone IIA analogs is reflected in their inhibition of tumor vascular endothelial cell proliferation, migration, and tube formation (29). However, it is still blank about the antitumor angiogenesis effect of SMART and its analogues so far. In this study, we first examined the anti-angiogenesis effect of **6h** by using *in vivo* and *in vitro* models. We prepared CM of NSCLC cells for subsequent experiments, aiming to simulate the tumor microenvironment (30). In the tube formation experiment, we found that the capillary-like structure formed by HMEC-1 pretreated with A549 or H460

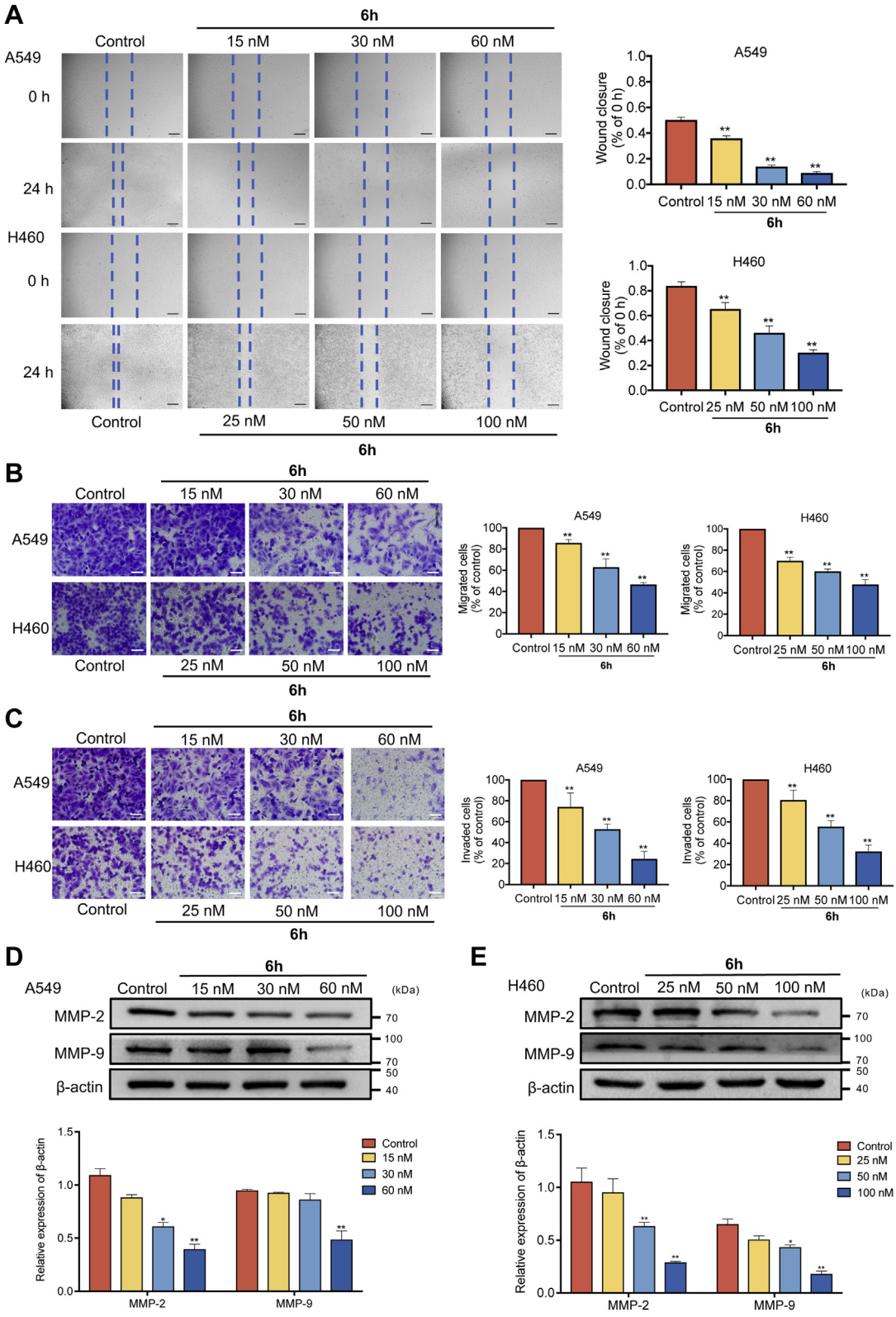

Figure 8. 6h represses the migration and invasion of A549 and H460 cells. *A*, cellular images of migratory recovery rate of A549 and H460 cells were photographed under an inverted microscope (the scale bar represents 200 μm). Treatment with **6h** inhibited the migration ability (*B*) and invasion ability (*C*) of A549 and H460 cells (the scale bar represents 50 μm). Both cells were added onto the upper chamber and incubated with the indicated concentrations of **6h**. Cells invading the lower surface of the membrane were detected by crystal violet staining. The expression changes of MMP-2 and MMP-9 were detected by Western blot in **6h**-treated A549 cells (*D*) and H460 cells (*E*). The histogram in each panel indicated the relative band intensity generated form densitometric scans of three independent experiments on arbitrary densitometric units. $^{*}p < 0.05$, $^{**}p < 0.01$ *versus* control. MMP, matrix metalloproteinase.

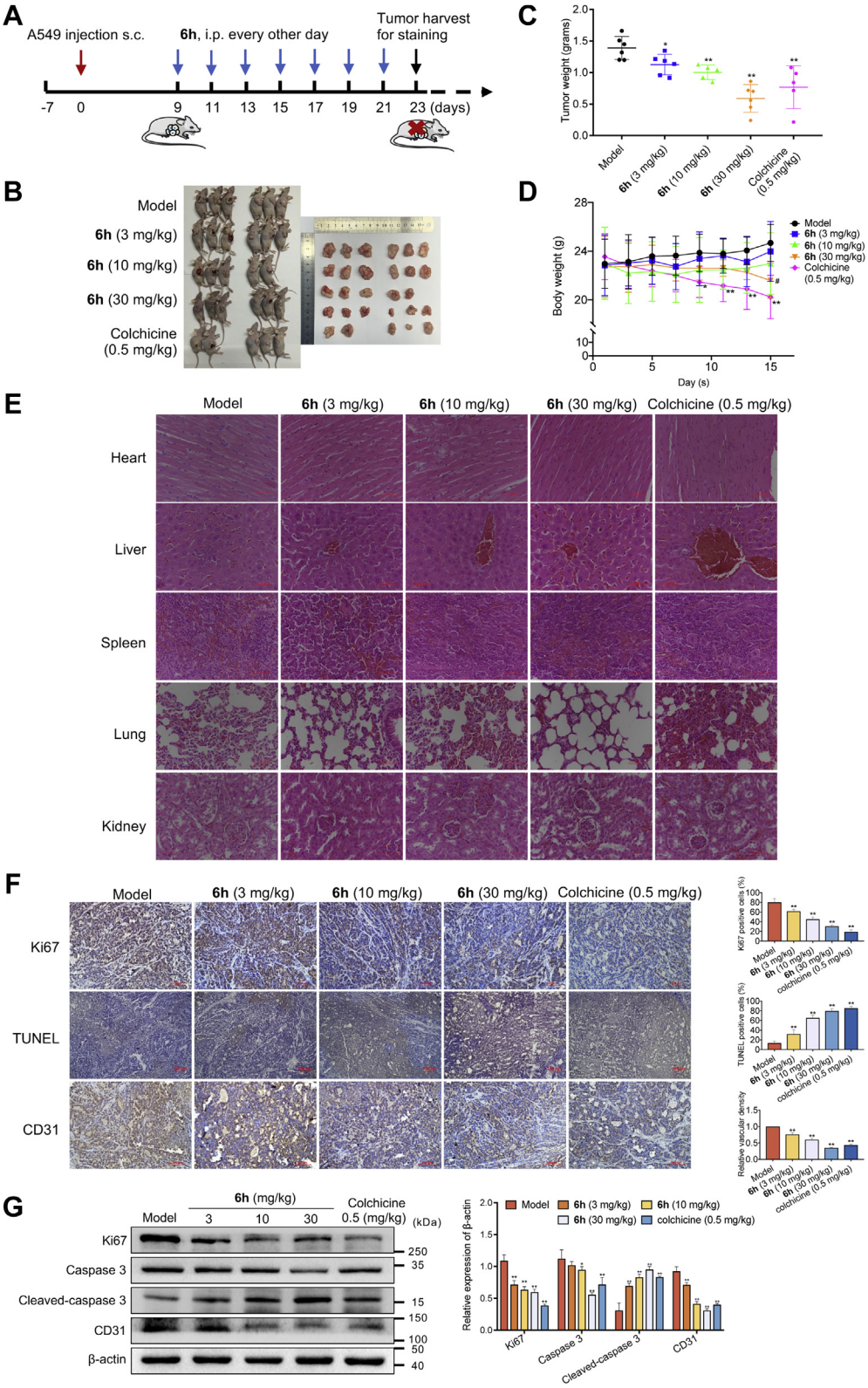

Figure 9. 6h induces a potent antitumor effect *in vivo*. *A*, flow chart of tumor-bearing mice treatment. BALB/c nude mice were inoculated subcutaneously with A549 cells (2×10^6) to establish transplanted tumor models. Once tumor volumes reached 200 mm^3, mice received i.p. injection every other day (seven times). After treatment, the xenograft tumors were taken out for weight and staining. *B*, images of BALB/c nude mice and resected A549 cell xenograft samples. *C*, average tumor weight at the end of indicated treatment. $*p < 0.05$, $**p < 0.01$ *versus* model group. *D*, the body weights of mice were measured during the indicated treatment. $**p < 0.01$ colchicine group *versus* model group. $\#p < 0.05$ **6h** (30 mg/kg) group *versus* model group. *E*, changes in histomorphology were evaluated of different tissues with HE staining. The scale bar represents 50 μm. *F*, representative immunohistochemistry images showing the expression of Ki67, CD31, and TUNEL-positive cells in the tumor tissues of tumor-bearing nude mice (*left*). The scale bar represents 100 μm. The percentage of positively stained cells and relative vascular density was quantified (*right*). $**p < 0.01$ *versus* model group. *G*, the expression of Ki67, caspase 3, cleaved-caspase 3, and CD31 of tumor tissues was detected by Western blot. The histogram in each panel indicated the relative band intensity generated form densitometric scans of three independent experiments on arbitrary densitometric units. $*p < 0.05$, $**p < 0.01$ *versus* model group.

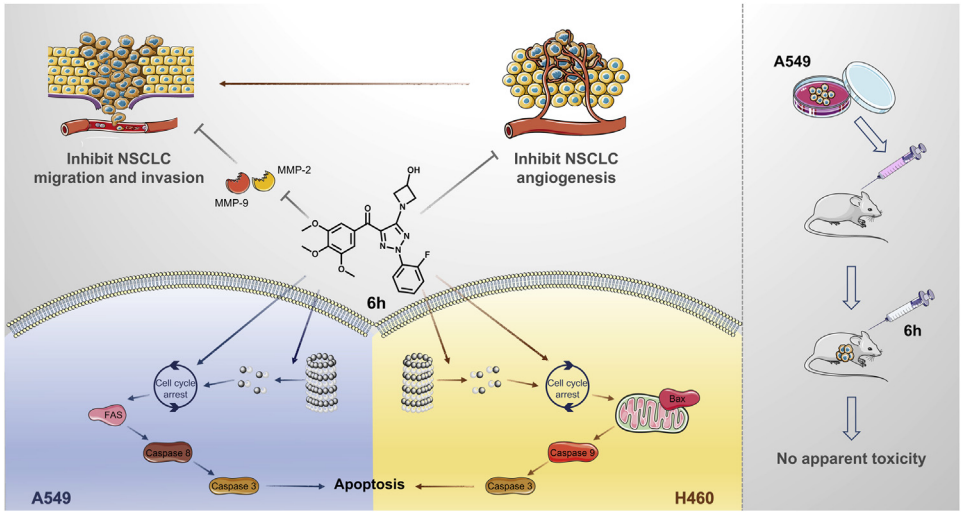

Figure 10. Schematic diagram of the mechanism of 6h against NSCLC. 6h, a novel tubulin inhibitor, exhibits antitumor effects and inhibits metastasis of NSCLC cells *via* targeting the tumor vascular system and inducing cell cycle arrest and apoptosis. Moreover, **6h** exhibits strong therapeutic efficacy *in vivo* without causing apparent toxicity by employing the NSCLC xenograft nude mouse model. NSCLC, non–small cell lung cancer.

CM is long and strong, and **6h** could effectively interfere with the formation of these tubular structures. In addition, the rat aortic ring experiment and the chicken embryo allantoic membrane experiment also proved that **6h** could prevent the formation of new blood vessels around the aortic ring and in the CAM induced by A549 or H460 CM. The aforementioned results suggest that **6h** is an effective antitumor angiogenesis agent.

After clarifying the antitumor angiogenesis effect, we focused on another major function of **6h**, microtubule depolymerization. We found that **6h** could exert excellent antiproliferative activity against a variety of tumor cells, especially on NSCLC cell lines, with IC_{50} mostly at the nanomolar level. *In vitro* tubulin polymerization test and immunofluorescence analysis proved that **6h** could inhibit tubulin polymerization. Microtubule inhibitors usually affect the cell cycle (31). In our study, **6h** evoked G2/M cell cycle arrest in A549 and H460 cells in time-dependent manners.

Apoptosis is mainly mediated by death receptor pathway (FAS/caspase 8/caspase 3), mitochondrial pathway (Bcl-2 family/caspase 9/caspase 3), and endoplasmic reticulum pathway, and the characteristic of this process is the continuous activation of caspase (32, 33). Our further results showed that **6h** time-dependently upregulated the expression of FAS in A549 cells, and subsequently activated caspase 8 and caspase 3, but had no effect on the expression of caspase 9 and Bax. We also observed the upregulation of cleaved-PARP and cleaved-caspase 3 in A549 cells, which suggested that **6h** induced A549 cell apoptosis through the death receptor pathway. The difference is that the apoptosis of H460 cells may be mediated by the mitochondrial pathway, which was confirmed by the activation of Bax, caspase 9, caspase 3, and the degradation of PARP protein without affecting the expression of caspase 8 and FAS after **6h** treatment. All the aforementioned results indicate that **6h** induces apoptosis of A549 and H460 cells.

Tumor angiogenesis can promote tumor cells to invade the blood system, thereby triggering tumor metastasis, which is one of the main obstacles to NSCLC treatment (34). Our results showed that **6h** could suppress the production of MMPs (MMP-2 and MMP-9), thereby inhibiting the migration and invasion of NSCLC cells (35). Furthermore, the *in vivo* experiments proved that the tumor growth of nude mice was effectively inhibited after **6h** treatment, and **6h** did not cause detectable pathological abnormality of main organs. Angiogenesis in tumors provides conditions for the growth and development of solid tumors (7). As we speculated previously, the *in vivo* results also confirmed that **6h** could reduce the microvessel density in tumor tissues of nude mice, which may be another important reason for inhibiting tumor growth.

In conclusion, the present study proved that 2-(2-fluorophenyl)-3-(3,4,5-trimethoxybenzoyl)-5-(3-hydroxyazetidin-1-yl)-2*H*-1,2,3-triazole (**6h**) is a newly designed and synthesized tubulin inhibitor targeting the colchicine-binding site with improved stability and aqueous solubility. **6h** exhibits significant antitumor effects and inhibits metastasis of NSCLC cells *via* targeting the tumor vascular system and inducing cell cycle arrest and apoptosis. Moreover, **6h** exhibits potent therapeutic efficacy *in vivo* as an antiangiogenic and antitumor agent without causing apparent toxicity. These findings provide convincing preclinical evidence to support **6h** as a candidate compound for the treatment of NSCLC.

Experimental procedures

Chemistry

All reagents and solvents required for chemical synthesis were obtained from commercial and were used without further purification. Analytical TLC had performed on silica gel plates and visualized by UV light (λ = 254 nm). Melting points were

recorded on a hot-stage microscope (Beijing Taike, X-4) and were not corrected. The ^{1}H-NMR spectra were recorded at 600 MHz or 400 MHz and recorded the ^{13}C-NMR spectra at 150 MHz or 100 MHz on a Bruker AVANCE. High-resolution mass spectra were performed using Agilent Accurate-Mass Q-TOF 6530 instrument in electrospray ionization mode. Specific synthetic methods of compounds are shown in the supporting information. And generated spectrums of **6a–6x** are shown in Figs. S1–S24.

Materials

RPMI1640 and Dulbecco's modified Eagle's medium were from Gibco. Endothelial cell medium (ECM) was obtained from ScienCell Research Laboratories. Fetal bovine serum (FBS) was purchased from TBD Biotechnology Development. MTT, 4′,6-diamidino-2-phenylindole, and PI were obtained from Sigma–Aldrich. Annexin V–FITC/PI was purchased from KeyGEN BioTECH. Hoechst 33258, bicinchoninic acid protein assay kit, and colorimetric TUNEL apoptosis assay kit were purchased from Beyotime Biotechnology. The Tubulin Polymerization Assay Kit was from Cytoskeleton. Primary antibodies against p53, PARP, FAS, Bax, β-actin, caspase 9, caspase 8, caspase 3, CD31, Ki67, MMP-2 and MMP-9, and FITC-conjugated secondary antibody were purchased from Santa Cruz Biotechnology. Horseradish peroxidase–conjugated secondary antibodies (goat–anti-rabbit and goat–antimouse) were purchased from ZSGB-BIO. Matrigel was from BD Biosciences.

Cell culture

The human NSCLC cell lines (A549, A549/Taxol, and H460), human breast carcinoma cell lines (MCF-7, MCF-7/ADM, and MDA-MB-231), human gastric adenocarcinoma cell line (SGC-7901), human liver cancer cell lines (HepG2 and BEL-7402), and human colonic adenocarcinoma cell line (HT-29) were purchased from American Type Culture Collection. Cells were cultured in RPMI1640 supplemented with 10% FBS and 1% penicillin/streptomycin. HMEC-1 was obtained from ScienCell Research Laboratories. HMEC-1 cells were maintained in ECM. All these cells were incubated in humidified atmosphere at 37 °C with 5% CO_2.

Animal studies

BALB/c nude mice (female and male, 4–6 weeks old) were available from Huafukang Experimental Animal Center. Sprague–Dawley rats (male, 4–6 weeks old, 150–180 g) were from Liaoning Changsheng Biotechnology Co, Ltd. All animals were kept in the Specific Pathogen Free Experimental Animal Center of Shenyang Pharmaceutical University and approved by the school animal experiment ethics committee. Every effort was made to minimize the suffering of animals.

Measurement of aqueous solubility

The solubility of test compounds was measured using the HPLC-UV method at pH 7.4 as described previously (36).

Cell viability

The effects of target compounds **6a–6x**, colchicines, and SMART on cell viability *in vitro* were performed by the MTT assay as previously described (37).

Tube formation assay

The 96-well plate was coated with 50 μl of Matrigel mixed with an equal volume of FBS-free medium, which was allowed to polymerize at 37 °C for 30 min. A549 cells or H460 cells were treated with various concentrations of **6h** for 24 h, and the CM from each group was collected. After being pretreated with ECM or ECM containing 50% CM for 24 h, HMEC-1 cells were inoculated on the Matrigel. After 6 h of incubation, the formation of tubes was observed using a Nikon C2 microscope.

Aortic ring assay

The aortic ring assay was performed as described (18). Briefly, the aortas that isolated from male Sprague–Dawley rats were cut into sections of 1 to 1.5 mm long rings and immersed in Matrigel in the 96-well plates individually. About 1 h later, the aortic rings were treated with 50 μl of regular medium (control) or regular medium containing 50% CM with **6h** and incubated at 37 °C for 7 days. The sprouted microvessels were observed and photographed using a Nikon C2 microscope.

CAM assay

The fertilized eggs were incubated in an incubator with a humidity of 65% at 37 °C for 7 days. Then, a window was carefully created at the top of the eggshell. After treating A549 cells or H460 cells with different concentrations of **6h**, the cell supernatant was collected and concentrated and then added to the embryo. The eggs were sealed with a transparent film and further incubated for 48 h. The microvessels in CAM were captured using a mobile phone (iPhone Xs Max).

Colony formation assay

Cells were plated in 6-well plates at 5000 cells/well and treated with **6h** for 48 h and then shifted into free-drug fresh medium for 2 weeks. When the cells have grown into visible colonies, crystal violet staining was performed according to the manufacturer's instructions and photographed by a digital camera (Canon).

Molecular docking

All the docking compounds were constructed by ChemDraw, optimized and saved by Chem3D, and then all the structures were imported into Schrödinger software to establish a database by using LigPrep (version 2.1.207). The crystal structure of tubulin (PDB ID: 1SA0) was from the PDB (http://www.rcsb.org/). And the protein structure was processed on Maestro 11.9 platform. The processing and optimization of virtual screening was completed by Glide module in Schrödinger Maestro software. Protein Preparation Wizard module was used for protein processing. All compounds were prepared

according to the default settings of LigPre module. When screening in Glide module, the prepared receptor was imported to specify the appropriate position in the receptor grid generation. Postures with good hydrogen bond geometry and a low energy conformation were selected. PyMOL (version 2.1, Schrödinger, Inc.) was used to draw figures.

In vitro *microtubule polymerization assay*

The Tubulin Polymerization Assay Kit was employed to characterize the effect of **6h** on microtubule polymerization as described previously (38). Briefly, the test compounds were incubated with tubulin protein in special reaction buffer. Absorbance (excitation = 370 nm, emission = 445 nm) was determined by a fluorescence plate reader (Varioskan. Flash).

Cell cycle analysis

The cell cycle analysis was performed with reference to the previously reported method (39). In brief, A549 or H460 cells were treated with colchicine or **6h** and fixed with 70% ethanol for at least 8 h. The samples were stained with PI and analyzed by FACScan flow cytometry (Becton–Dickinson).

Apoptosis assay

The morphological changes of apoptotic cell nuclei were evaluated by Hoechst 33258 staining. Apoptosis assay was performed as described previously (40). Cells were processed according to the operating instructions of the annexin V–FITC/PI staining kit. The samples were detected by a Nikon C2 microscope or FACS. Apoptosis rate (%) = early apoptosis rate (PI^-; annexin $V–FITC^+$) + late apoptosis rate (PI^+; annexin $V–FITC^+$).

Western blot analysis

Western blot was performed as previously reported (40). The ImageJ software (National Institutes of Health) was used for absorbance measurement.

Immunofluorescence and immunohistochemistry assay

The routine procedure is operated to perform immunofluorescence staining to observe the microtubule morphology of the cells, which were seeded into glass bottom cell culture dishes with a specified concentration of colchicine or **6h** for 24 h. After fixation with paraformaldehyde for 30 min, cells were permeabilized with 0.2% Triton X-100 for 30 min. Next, cells were blocked with 5% bovine serum albumin for 30 min and were incubated with the anti–α-tubulin primary antibody overnight. And cells were incubated with FITC-conjugated secondary antibody for 2 h at room temperature. The nuclei were stained with 4′,6-diamidino-2-phenylindole for another 20 min. For immunohistochemistry studies, the stain of tumor tissues was visualized by 3,3-diaminobenzidine and Harris hematoxylin. Apoptotic cells induced by **6h** or colchicine in the tumor tissues were detected by Colorimetric TUNEL Apoptosis Assay Kit, in accordance with the manufacturer's protocol. The immunofluorescence and immunohistochemistry were observed by a confocal microscopy (Nikon C2).

Wound-healing assay

Cells (4×10^5/well) were planted and cultured in a 6-well plate for 24 h. Monolayer cells were wounded by a sterilized 200-μl pipette tip. After being washed with PBS for three times, the cells were imaged as control groups. Then cells were treated with specified concentration of **6h** for 24 h and observed using a Nikon C2 microscope.

Migration and invasion assay

Migration and invasion assays were performed as described previously (41). Transwell chambers (8 μM pore size; Corning) were used with or without 50 μl Matrigel (Matrigel:Dulbecco's modified Eagle's medium = 1:8) to test the invasion or migration ability of A549 or H460 cells. A Nikon C2 microscope was used to take pictures.

In vivo *mouse xenograft assay*

A549 cells (2×10^6) were inoculated subcutaneously in the right axilla of BALB/c nude mice to establish transplanted tumor models, with 0.2 ml of serum-free media as the vehicle. Once tumor volumes (length × $width^2$/2) reached 200 mm^3, the mice were randomly divided into five groups (n = 6): model group (vehicle, 5% ethanol + 20% PEG-400 + 75% saline), **6h**-treated groups (3, 10, and 30 mg/kg), and colchicine group (0.5 mg/kg). The mice received i.p injection every other day for seven times. After treatment, xenograft tumors were taken out, weighted, and photographed.

H&E staining

Main organs from BALB/c nude mice were fixed and embedded. Paraffin sections (5 μm thick) were stained with H&E according to the standard procedure as described (42). The images were taken with a light microscope (Olympus).

Statistics analysis

Data were shown as mean ± SD, and all *in vitro* experiments were independently performed at least three times. Comparisons among multiple groups were determined using one-way ANOVA followed by least significant difference test. A value of $p < 0.05$ was defined as statistically significant.

Data availability

All relevant data are within the article and its supporting information files.

Supporting information—This article contains supporting information.

Acknowledgments—We gratefully acknowledge the funding from the National Natural Science Foundation of China (grant numbers: 81872394 and 81602969); the Natural Science Foundation of Liaoning Province of China (grant number: 2020-MS-187); the

Innovative Talents Support Plan of Colleges and Universities in Liaoning Province (grant number: LR2020080); and the Innovation and Entrepreneurship Training Program of Shenyang Pharmaceutical University (grant number: 202010163004) for the generous financial support.

Author contributions—W. Z. and D. Z. conceptualization; T. Z. and X. C. validation; Z. L., L. H., T. Z., M. H., and Q. G. formal analysis; Z. L., L. H., X. C., Y. Y., Y. S., Z. L., and Y. W. investigation; Z. L. and Q. G. data curation; Z. L., W. Z., and D. Z. writing–original draft; D. Z. writing–review & editing; Z. L. and Q. G. visualization; W. Z. and D. Z. supervision.

Conflict of interest—The authors declare that they have no conflicts of interest with the contents of this article.

Abbreviations—The abbreviations used are: CAM, chicken chorioallantoic membrane; CM, conditioned medium; ECM, endothelial cell medium; FBS, fetal bovine serum; HMEC, human microvascular endothelial cell line; MMP, matrix metalloproteinase; MTT, 3-(4,5-dimethylthiazol-2-yl)-2,5-diphenyl-2H-tetrazolium bromide; NSCLC, non–small cell lung cancer; PARP, poly(ADP-ribose) polymerase; PDB, Protein Data Bank; PI, propidium iodide; SMART, 4-substituted methoxybenzoyl-aryl-thiazole.

References

1. Khan, P., Siddiqui, J. A., Lakshmanan, I., Ganti, A. K., Salgia, R., Jain, M., *et al.* (2021) RNA-based therapies: a cog in the wheel of lung cancer defense. *Mol. Cancer* **20**, 54
2. Makhov, P., Bychkov, I., Faezov, B., Deneka, A., Kudinov, A., Nicolas, E., *et al.* (2021) Musashi-2 (MSI2) regulates epidermal growth factor receptor (EGFR) expression and response to EGFR inhibitors in EGFR-mutated non-small cell lung cancer (NSCLC). *Oncogenesis* **10**, 29
3. Liu, Y., Chen, P., Wang, H., Wu, S., Zhao, S., He, Y., *et al.* (2021) The landscape of immune checkpoints expression in non-small cell lung cancer: a narrative review. *Transl. Lung Cancer Res.* **10**, 1029–1038
4. Li, Q., Yu, D., Yu, Z., Gao, Q., Chen, R., Zhou, L., *et al.* (2021) TIPE3 promotes non-small cell lung cancer progression *via* the protein kinase B/extracellular signal-regulated kinase 1/2-glycogen synthase kinase 3β-β-catenin/Snail axis. *Trans. Lung Cancer Res.* **10**, 936–954
5. Hartmann, O., Reissland, M., Maier, C. R., Fischer, T., Prieto-Garcia, C., Baluapuri, A., *et al.* (2021) Implementation of CRISPR/Cas9 genome editing to generate murine lung cancer models that depict the mutational landscape of human disease. *Front. Cell Dev. Biol.* **9**, 641618
6. Zhu, B., V, M., Finch-Edmondson, M., Lee, Y., Wan, Y., Sudol, M., *et al.* (2021) miR-582-5p is a tumor suppressor microRNA targeting the hippo-YAP/TAZ signaling pathway in non-small cell lung cancer. *Cancers* **13**, 756
7. Daum, S., Hagen, H., Naismith, E., Wolf, D., and Pircher, A. (2020) The role of anti-angiogenesis in the treatment landscape of non-small cell lung cancer - new combinational approaches and strategies of neovessel inhibition. *Front. Cell Dev. Biol.* **8**, 610903
8. Gao, Q., Tang, S., Chen, H., Chen, H., Li, X., Jiang, Y., *et al.* (2020) Intratumoral injection of anlotinib hydrogel enhances antitumor effects and reduces toxicity in mouse model of lung cancer. *Drug Deliv.* **27**, 1524–1534
9. Sun, M., Zhang, Y., Qin, J., Ba, M., Yao, Y., Duan, Y., *et al.* (2021) Synthesis and biological evaluation of new 2-methoxyestradiol derivatives: potent inhibitors of angiogenesis and tubulin polymerization. *Bioorg. Chem.* **113**, 104988
10. Yang, M., Su, Y., Wang, Z., Du, D., Wei, S., Liao, Z., *et al.* (2021) C118P, a novel microtubule inhibitor with anti-angiogenic and vascular disrupting activities, exerts anti-tumor effects against hepatocellular carcinoma. *Biochem. Pharmacol.* **190**, 114641
11. McLoughlin, E. C., and O'Boyle, N. M. (2020) Colchicine-binding site inhibitors from chemistry to clinic: a review. *Pharmaceuticals (Basel)* **13**, 8
12. Gallego-Yerga, L., Ochoa, R., Lans, I., Peña-Varas, C., Alegría-Arcos, M., Cossio, P., *et al.* (2021) Application of ensemble pharmacophore-based virtual screening to the discovery of novel antimitotic tubulin inhibitors. *Comput. Struct. Biotec.* **19**, 4360–4372
13. Lu, Y., Li, C. M., Wang, Z., Ross, C. R., 2nd, Chen, J., Dalton, J. T., *et al.* (2009) Discovery of 4-substituted methoxybenzoyl-aryl-thiazole as novel anticancer agents: synthesis, biological evaluation, and structure-activity relationships. *J. Med. Chem.* **52**, 1701–1711
14. Li, C. M., Wang, Z., Lu, Y., Ahn, S., Narayanan, R., Kearbey, J. D., *et al.* (2011) Biological activity of 4-substituted methoxybenzoyl-aryl-thiazole: an active microtubule inhibitor. *Cancer Res.* **71**, 216–224
15. Wang, S.-F., Yin, Y., Zhang, Y.-L., Mi, S.-W., Zhao, M.-Y., Lv, P.-C., *et al.* (2015) Synthesis, biological evaluation and 3D-QSAR studies of novel 5-phenyl-1H-pyrazol cinnamamide derivatives as novel antitubulin agents. *Eur. J. Med. Chem.* **93**, 291–299
16. Liang, H., Ge, F., Xu, Y., Xiao, J., Zhou, Z., Liu, R., *et al.* (2018) miR-153 inhibits the migration and the tube formation of endothelial cells by blocking the paracrine of angiopoietin 1 in breast cancer cells. *Angiogenesis* **21**, 849–860
17. Stryker, Z. I., Rajabi, M., Davis, P. J., and Mousa, S. A. (2019) Evaluation of angiogenesis assays. *Biomedicines* **7**, 37
18. Huang, Y., Fang, J., Lu, W., Wang, Z., Wang, Q., Hou, Y., *et al.* (2019) A systems pharmacology approach uncovers wogonoside as an angiogenesis inhibitor of triple-negative breast cancer by targeting hedgehog signaling. *Cell Chem. Biol.* **26**, 1143–1158.e1146
19. Nicosia, R. F. (2009) The aortic ring model of angiogenesis: a quarter century of search and discovery. *J. Cell Mol. Med.* **13**, 4113–4136
20. Kundekova, B., Macajova, M., Meta, M., Cavarga, I., and Bilcik, B. (2021) Chorioallantoic membrane models of various avian species: differences and applications. *Biology (Basel)* **10**, 301
21. Harper, K., Yatsyna, A., Charbonneau, M., Brochu-Gaudreau, K., Perreault, A., Jeldres, C., *et al.* (2021) The chicken chorioallantoic membrane tumor assay as a relevant *in vivo* model to study the impact of hypoxia on tumor progression and metastasis. *Cancers (Basel).* **13**, 1093
22. Nowak-Sliwinska, P., Segura, T., and Iruela-Arispe, M. L. (2014) The chicken chorioallantoic membrane model in biology, medicine and bioengineering. *Angiogenesis* **17**, 779–804
23. Cao, Y., Wang, J., Tian, H., and Fu, G. H. (2020) Mitochondrial ROS accumulation inhibiting JAK2/STAT3 pathway is a critical modulator of CYT997-induced autophagy and apoptosis in gastric cancer. *J. Exp. Clin. Cancer Res.* **39**, 119
24. Li, W., Yin, Y., Shuai, W., Xu, F., Yao, H., Liu, J., *et al.* (2019) Discovery of novel quinazolines as potential anti-tubulin agents occupying three zones of colchicine domain. *Bioorg. Chem.* **83**, 380–390
25. Pagano, E., Venneri, T., Lucariello, G., Cicia, D., Brancaleone, V., Nanì, M. F., *et al.* (2021) Palmitoylethanolamide reduces colon cancer cell proliferation and migration, influences tumor cell cycle and exerts *in vivo* chemopreventive effects. *Cancers* **13**, 1923
26. Pal, J., Becker, A. C., Dhamija, S., Seiler, J., Abdelkarim, M., Sharma, Y., *et al.* (2021) Systematic analysis of migration factors by MigExpress identifies essential cell migration control genes in non-small cell lung cancer. *Mol. Oncol.* **15**, 1797–1817
27. Xiong, Y., He, L., Shay, C., Lang, L., Loveless, J., Yu, J., *et al.* (2019) Nck-associated protein 1 associates with HSP90 to drive metastasis in human non-small-cell lung cancer. *J. Exp. Clin. Cancer Res.* **38**, 122
28. Feng, D., Wu, Y., Wang, H., Bai, Z., Wang, D., Zuo, D., *et al.* (2017) Synthesis and antiproliferative activity of 2-aryl-4-(3,4,5-trimethoxybenzoyl)-1,2,3-triazol derivatives as microtubule-destabilizing agents. *RSC Adv.* **7**, 29103–29111
29. Huang, H., Yao, Y., Hou, G., Zhao, C., Qin, J., Zhang, Y., *et al.* (2021) Design, synthesis and biological evaluation of tanshinone IIA-based analogues: potent inhibitors of microtubule formation and angiogenesis. *Eur. J. Med. Chem.* **224**, 113708

30. Jin, S., Yang, C., Huang, J., Liu, L., Zhang, Y., Li, S., *et al.* (2020) Conditioned medium derived from FGF-2-modified GMSCs enhances migration and angiogenesis of human umbilical vein endothelial cells. *Stem Cell Res. Ther.* **11**, 68
31. Shuai, W., Li, X., Li, W., Xu, F., Lu, L., Yao, H., *et al.* (2020) Design, synthesis and anticancer properties of isocombretapyridines as potent colchicine binding site inhibitors. *Eur. J. Med. Chem.* **197**, 112308
32. Xiang, L., He, B., Liu, Q., Hu, D., Liao, W., Li, R., *et al.* (2020) Antitumor effects of curcumin on the proliferation, migration and apoptosis of human colorectal carcinoma HCT116 cells. *Oncol. Rep.* **44**, 1997–2008
33. Zhang, J., Zhou, L., Nan, Z., Yuan, Q., Wen, J., Xu, M., *et al.* (2017) Knockdown of cMyc activates Fas-mediated apoptosis and sensitizes A549 cells to radiation. *Oncol. Rep.* **38**, 2471–2479
34. Wood, S. L., Pernemalm, M., Crosbie, P. A., and Whetton, A. D. (2014) The role of the tumor-microenvironment in lung cancer-metastasis and its relationship to potential therapeutic targets. *Cancer Treat Rev.* **40**, 558–566
35. Song, J. H., Park, J., Park, S. L., Hwang, B., Kim, W. J., Lee, C., *et al.* (2021) A novel cyclic pentadepsipeptide, N-methylsansalvamide, suppresses angiogenic responses and exhibits antitumor efficacy against Bladder cancer. *Cancers (Basel).* **13**, 191
36. Huang, L., Liu, M., Man, S., Ma, D., Feng, D., Sun, Z., *et al.* (2020) Design, synthesis and bio-evaluation of novel 2-aryl-4-(3,4,5-trimethoxy-benzoyl)-5-substituted-1,2,3-triazoles as the tubulin polymerization inhibitors. *Eur. J. Med. Chem.* **186**, 111846
37. Shen, J., Wang, J., Du, J., Wang, L., Zhou, X., Chang, X., *et al.* (2019) A novel ALK inhibitor ZYY inhibits Karpas299 cell growth *in vitro* and in a mouse xenograft model and induces protective autophagy. *Toxicol. Appl. Pharm.* **383**, 114781
38. Liu, Z., Lang, B., Gao, M., Chang, X., Guan, Q., Xu, Q., *et al.* (2020) 3-(3-Methoxyphenyl)-6-(3-amino-4-methoxyphenyl)-7H-[1,2,4] triazolo [3,4-b][1,3,4] thiadiazine, a novel tubulin inhibitor, evokes G2/M cell cycle arrest and apoptosis in SGC-7901 and HeLa cells. *J. Cell Biochem.* **121**, 2184–2196
39. Bai, Z., Gao, M., Zhang, H., Guan, Q., Xu, J., Li, Y., *et al.* (2017) BZML, a novel colchicine binding site inhibitor, overcomes multidrug resistance in A549/Taxol cells by inhibiting P-gp function and inducing mitotic catastrophe. *Cancer Lett.* **402**, 81–92
40. Li, L., Cui, J., Liu, Z., Zhou, X., Li, Z., Yu, Y., *et al.* (2018) Silver nanoparticles induce SH-SY5Y cell apoptosis *via* endoplasmic reticulum- and mitochondrial pathways that lengthen endoplasmic reticulum-mitochondria contact sites and alter inositol-3-phosphate receptor function. *Toxicol. Lett.* **285**, 156–167
41. Zheng, D., Chang, X., Liu, Y., Xu, J., Gou, W., Li, Z., *et al.* (2018) 2-Methoxy-5((3,4,5-trimethosyphenyl)seleninyl) phenol reverses EGF-induced cell migration and invasion through down-regulation of MDM2 in breast cancer cell lines. *Cancer Biol. Ther.* **20**, 513–523
42. Chen, H., Deng, S., Wang, Y., Albadari, N., Kumar, G., Ma, D., *et al.* (2019) Structure–activity relationship study of novel 6-Aryl-2-benzoylpyridines as tubulin polymerization inhibitors with potent antiproliferative properties. *J. Med. Chem.* **63**, 827–846